GSA DATA REPOSITORY 2014357 Maxbauer et al.

APPENDIX DR1. AGE CONSTRAINTS FOR NAPARTULIK SITE

Several lines of evidence support a middle Eocene age for the Napartulik forest site (Fig. DR1). Both Ricketts (1986) and Miall (1986) considered the Buchanan Lake Formation middle to late Eocene in age based on lithostratigraphic correlation. Miall (1986) proposed that deposition of the Buchanan Lake Formation may have continued into the early Oligocene, although there is no additional evidence to support a post-Eocene age (Basinger, 1991). The palynofloral assemblages are most similar to other middle Eocene Arctic palynofloras; however, a late Eocene age cannot be dismissed (McIntyre, 1991; Ricketts and McIntyre, 1986). A middle Eocene age is strongly supported by the discovery of a brontothere tooth comparable to similar genera known from other Arctic deposits of Uintan to Duchesnean North American Land Mammal Ages (NALMA; 47.9-37.8 Ma; Eberle and Storer, 1999).

Harrison et al. (1999) correlated Cenozoic strata across the Canadian Arctic and Greenland and placed the Buchanan Lake Formation in their Cenozoic Sequence 6, dated 47.8-41.2 Ma (Lutetian/Uintan, C19 to C21 on the magnetic time scale, originally presented as 47.5-41.3 Ma; updated here following Gradstein et al. (2012)). Their evidence is based largely on the palynofloral work of McIntyre (1991) and the brontothere index fossil from Eberle and Storer (1999), with additional weak evidence from correlated volcanic activity in other regions of Canada. Importantly, Harrison et al. (1999) do not present a clear or compelling case for excluding 41.2-37.8 Ma from the possible age range of Napartulik.

Following Eberle and Storer (1999) and Harrison et al. (1999), many studies have adopted an age of "~45 Ma" for Napartulik (e.g., Jahren, 2007; Jahren et al., 2009; Jahren and Sternberg, 2008; Wang and Leng, 2011; Yang et al., 2005). This age is near the old end of all published age ranges for the site, and is therefore somewhat misleading. Other studies have adopted the age range presented by Harrison et al. (1999) (e.g., Eberle and Greenwood, 2012; Jahren et al., 2004; Richter and LePage, 2005; Williams et al., 2003) and ignore the possibility of a younger age accommodated by the brontothere tooth. Here we adopt the most conservative age range of 47.9-37.8 Ma.

The fossil-bearing lignite horizons are estimated to have accumulated at a rate of 0.8 mm yr^{-1} (Greenwood and Basinger, 1993; Kojima et al., 1998). Considering the total thickness of the six lignite layers where our CO_2 estimates come from (~2.35 m; see Fig. DR2), the time required to deposit these forests is ~2,938 yrs. Assuming the remaining deposits formed under constant sedimentation rates of 10,106 yrs m^{-1} for the siltstones and sandy siltstones (~16.96 m), and 2,495 yrs m^{-1} for the sandstones (2.64 m; based on sedimentation rates of generic floodplain soils and swamp sandstones, respectively; see Kleiss, 1996, after adjustment for density differences between Napartulik sandstone (2.0 g cm^{-3}) and a generic silty loam (1.5 g cm^{-3})), an approximate duration for our study section is ~181,000 yrs. It is worth noting that alternative stratigraphic sections exist for the Napartulik site (e.g., Jahren et al., 2009). The thickness of individual forest horizons varies laterally, and therefore discrepancy exists between the stratigraphic thicknesses presented here (Fig. DR2) and those presented by Jahren et al. (2009). However, for our study

section (F-B') the total thickness varies by ~2 m and the coal thickness varies only ~0.1 m, increasing our confidence that the presented age duration for this section is reasonable.

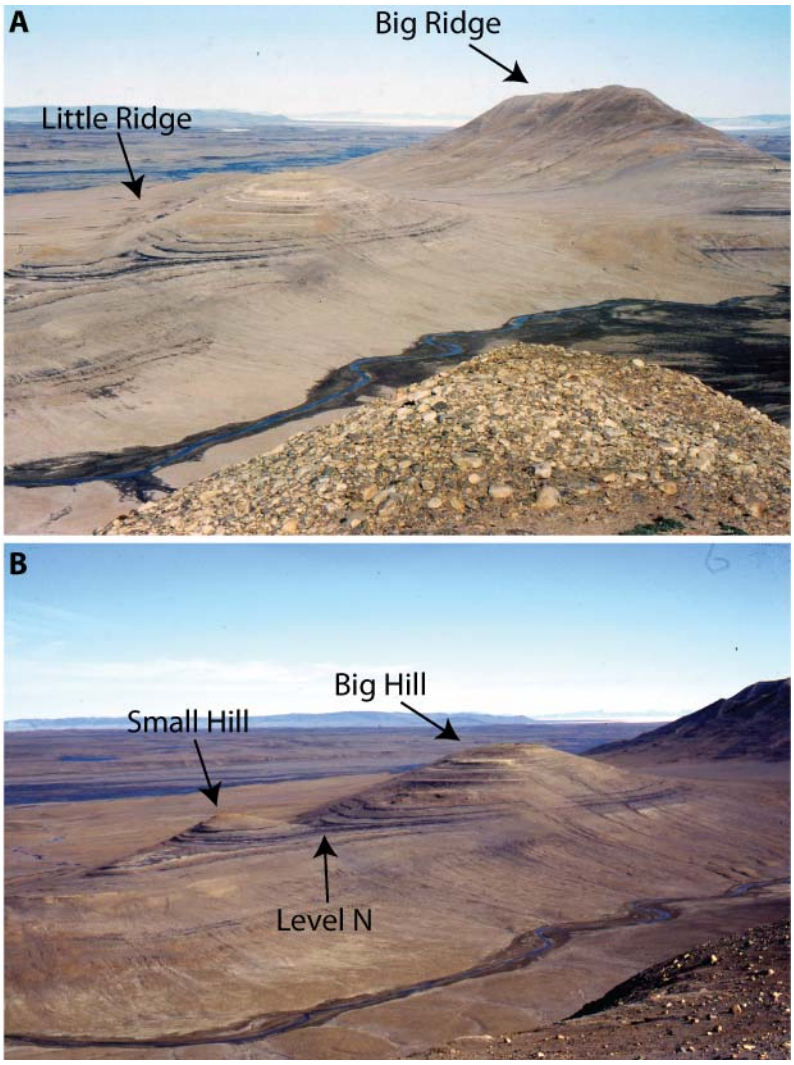

Figure DR1. Overview of the Napartulik site. **A.** Image showing Big Ridge and Little Ridge. Dark lignite layers are visible cropping out along the Little Ridge. Note that both "prime" and "non-prime" layers are found on the Big Ridge while the "non-prime" layers are only found on the Little Ridge (see Fig. DR2). **B.** Image showing the Little Ridge differentiating between the Big Hill and the Small Hill. Fossil forest level N forms the saddle between hills and has been the most intensely-investigated layer.

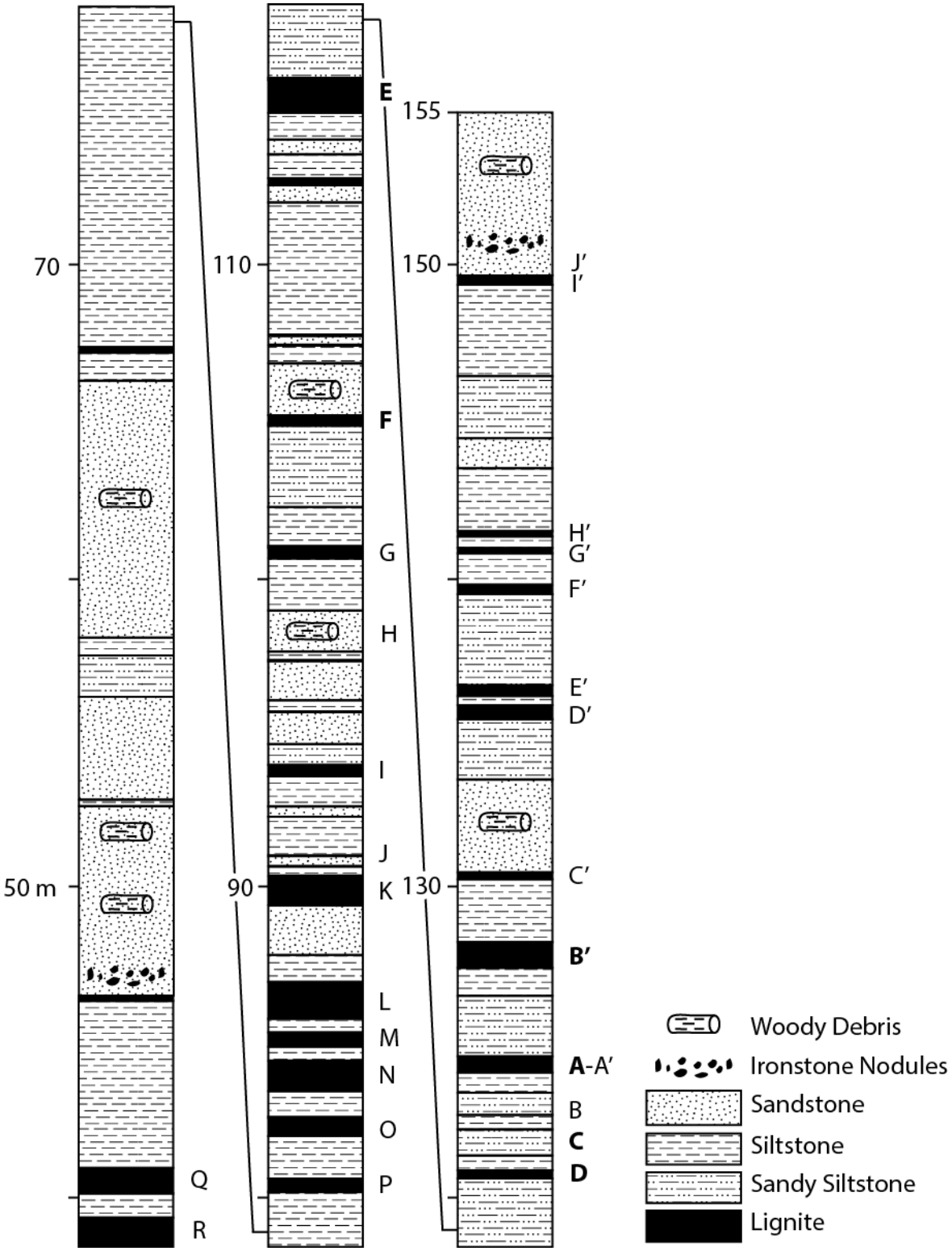

Figure DR2. Stratigraphic section for the Napartulik fossil forest site (adapted from LePage, 1993). The Little Ridge contains layers A-U; the Big Ridge contains layers A-E and A'-I' (see Fig. DR1). Eighteen layers were investigated in this study (Q-B'); CO_2 reconstructions come from the six layers indicated in bold (F-C, A, and B'), where the quality of cuticle preservation was sufficiently high.

APPENDIX DR2. METHODS FOR RECONSTRUCTING CO_2

DR2.1. Gas-exchange model

Recent developments in physiological models of plant gas exchange manipulate well-established photosynthetic theory into applicable methods for reconstructing atmospheric CO_2 (Franks et al., 2014; Konrad et al., 2008). The following is a summary of the Franks et al. (2014) model; application of a related gas-exchange model by Konrad et al. (2008), which also has been applied to the fossil record (Erdei et al., 2012; Grein et al., 2011, 2013), was unsuccessful here. Both models are specific to C_3 photosynthesis.

A well-validated relationship describes photosynthetic rate, A, in terms of total leaf conductance, $g_{c(tot)}$, and the difference between atmospheric CO_2 (C_a) and the concentration of CO_2 inside the leaf (C_i) (see Table DR1 for definitions and units of variables; Farquhar and Sharkey, 1982):

$$A = g_{c_{(tot)}}(C_a - C_i) \qquad \text{(DR1)}$$

Both a high capacity for gas exchange (i.e., conductance) and a strong depletion of CO_2 inside the leaf (i.e., large $C_a - C_i$) are associated with high A, and vice-versa at low A. Solving eq. (1) for C_a yields:

$$C_a = \frac{A}{\left[g_{c_{(tot)}}\left(1-{C_i}/{C_a}\right)\right]} \qquad \text{(DR2)}$$

This expression shows that changes in A impact C_a, unless those changes are counterbalanced by variations in $g_{c(tot)}$ or the C_i/C_a ratio (Franks et al., 2014). Assuming this physiological relationship holds true in the past, measurements of C_i/C_a and $g_{c(tot)}$, combined with some knowledge of A, can be used to reconstruct ancient C_a.

The C_i/C_a ratio is readily determined from the $\delta^{13}C$ of leaves (both living and fossil) using the well-documented relationship (Farquhar et al., 1982, 1989):

$$\frac{C_i}{C_a} = \frac{\Delta_{leaf} - a}{b - a} \qquad \text{(DR3)}$$

where Δ_{leaf} is the net carbon isotope discrimination by the leaf (in parts per thousand, ‰), a is the discrimination due to CO_2 diffusivity in air (4.4‰), and b is the discrimination due to the enzyme rubisco (30‰). Δ_{leaf} is related to the difference between the $\delta^{13}C$ of the leaf and atmosphere (Farquhar and Richards, 1984):

$$\Delta_{leaf} = \frac{\delta^{13}C_{air} - \delta^{13}C_{leaf}}{1 + \delta^{13}C_{leaf}/1000} \qquad \text{(DR4)}$$

The $\delta^{13}C$ of leaves and the atmosphere are determined relative to a standard (typically the Vienna Pee Dee Belemite, VPDB):

$$\delta^{13}C = \left(\frac{R_{sample}}{R_{standard}} - 1\right) \times 1000 \qquad \text{(DR5)}$$

where R is the ratio of $^{13}C/^{12}C$ (e.g., Farquhar et al., 1989).

Operational stomatal conductance, $g_{c(op)}$, cannot be directly measured from fossils, however it can be scaled from maximum stomatal conductance ($g_{c(max)}$). Environmental stress causes plants to operate below maximum photosynthetic capacity, accordingly $g_{c(op)}$ is typically some fraction of $g_{c(max)}$, ξ, that is usually between 0.3-0.5, but it is often lower when conditions are unfavorable (Franks et al., 2009, 2014). An expression for $g_{c(max)}$ is given as (Franks and Beerling, 2009b):

$$g_{c(\max)} = \frac{\frac{d}{v} \times D \times a_{max}}{\left(l + \frac{\pi}{2}\sqrt{\frac{a_{max}}{\pi}}\right)} \qquad \text{(DR6)}$$

where d and v are the constants that correspond to the diffusivity of CO_2 in air and the molar volume of air, respectively, l is stomatal pore depth, D is stomatal density, and a_{max} is the maximum stomatal aperture. Both a_{max} and l can be reliably modeled from guard cell length, a variable that is directly measurable on most cuticle-bearing fossils (*Metasequoia* is an exception; see section DR2.3) and that scales well with pore length (p) and single guard cell width (GCW). Assuming a circular cross-section for guard cells when fully inflated, $GCW = l$ (Franks and Beerling, 2009a); a_{max} is computed from p, $a_{max} = \beta \times \pi \times (p/2)^2$, where β is a scalar that describes how circular the stomatal pore is when fully open (Franks et al., 2014). Additional knowledge of GCW, when measurable, can improve estimates of a_{max} and l (Franks and Beerling, 2009b; Franks et al., 2014).

In addition to $g_{c(op)}$ (given as $\xi g_{c(max)}$), $g_{c(tot)}$ includes the mesophyll (g_{cm}) and boundary layer (g_{cb}) conductance, which correspond to diffusive resistivity through the assimilating tissue and airflow near the leaf surface, respectively. An expression for $g_{c(tot)}$ is given by (Franks et al., 2014; Jones, 1992):

$$g_{c_{(tot)}} = \left(\frac{1}{\xi g_{c(max)}} + \frac{1}{g_{cm}} + \frac{1}{g_{cb}}\right)^{-1} \qquad \text{(DR7)}$$

The final parameter required for calculating C_a using eq. (2) is A, the typical operational photosynthetic rate. This parameter obviously cannot be directly determined from fossils, therefore an approximate value is determined from a closely related extant taxon (if no close extant relative is available, the present-day global average value of 6.7 μmol m^{-2} s^{-1} can be used; Franks et al., 2014). Additionally, because A is influenced by C_a, the present-day value (A_0) may not be appropriate for fossil applications. To reconcile this problem, Franks et al. (2014) solve eq. (2) iteratively with the following equation relating A to C_a:

$$A = A_0 \left[\frac{(C_a - \Gamma^*)(C_{a0} + 2\Gamma^*)}{(C_a + 2\Gamma^*)(C_{a0} - \Gamma^*)}\right] \qquad \text{(DR8)}$$

where C_{a0} is the CO_2 value used for determining A_0 and Γ^* is the CO_2 compensation point in the absence of dark respiration (Franks et al., 2014). A generic value for Γ^* of 40 μmol mol^{-1} is used in the model and is based on an assumed leaf temperature during photosynthesis of 25 °C

(Franks et al., 2014; Helliker and Richter, 2008; Song et al., 2011). Most leaf productivity occurs within a narrow range of leaf temperature (~20-25 °C; Helliker and Richter, 2008), which importantly is not the same as ambient air temperature; air temperature varies much more strongly across latitudes than leaf temperature. If our assumed leaf temperature of 25 °C is too warm, this will cause an artificially high reconstruction of *A* and lead to an overestimation of CO_2. And additional complication in respect to our work is the potential influence of Arctic light regimes on photosynthetic activity. Currently, it is very poorly understood what influence photoperiod has on this system and should be the focus of future studies.

The accuracy (proximity of modeled CO_2 to known CO_2) of the model for reconstructing present-day CO_2 is as good or better than other leading CO_2 proxies (Franks et al., 2014). Further, precision in the model is fairly stable (~+35% and -25% of the median estimated CO_2 at 95% confidence), even at high CO_2 (Franks et al., 2014). This level of precision is as good or better than most other CO_2 proxies, particularly at high CO_2. A sensitivity analysis using the data reported here for Napartulik fossils and extant *M. glyptostroboides* (methods for reconstructions are described in sections DR2.2 and DR2.3) demonstrate that variation in each of the input parameters has a variable effect on estimated CO_2 (Fig. DR3). Estimated CO_2 is most strongly affected by D, $g_{c(op)}/g_{c(max)}$, A, and p, but is less sensitive to variation in l, g_{cm}, and g_{cb} (Fig. DR3).

All estimates were derived using the R code for the model provided in Franks et al. (2014).

Table DR1. List of all input parameters related to stomatal geometry and physiology.

Symbol	Definition	Unit
Stomatal Geometry		
p	pore length	μm
GCW	single guard cell width	μm
IRL	inner rectangular length	μm
a_{max}	maximum stomatal aperture	μm^2
l	stomatal pore depth	μm
D	stomatal density	μm^2
SI	stomatal index	%
Physiology		
$g_{c(op)}$	operational stomatal conductance to CO_2	mol m^{-2} s^{-1}
$g_{c(max)}$	maximum stomatal conductance to CO_2	mol m^{-2} s^{-1}
ξ or $g_{c(op)}/g_{c(max)}$	ratio of operational to maximum stomatal conductance	
g_{cm}	mesophyll conductance to CO_2	mol m^{-2} s^{-1}
g_{cb}	boundary layer conductance to CO_2	mol m^{-2} s^{-1}
$g_{c(tot)}$	total operational leaf conductance to CO_2	mol m^{-2} s^{-1}
A	photosynthetic rate	μmol m^{-2} s^{-1}
A_o	photosynthetic rate at 360 ppm CO_2	μmol m^{-2} s^{-1}
C_a	concentration of atmospheric CO_2	ppmV
C_i	concentration of CO_2 within the leaf	ppmV
C_i/C_a	ratio of internal to ambient CO_2 concentration	
Δ_{leaf}	net carbon isotope fractionation by the leaf	‰
$\delta^{13}C_{leaf}$	carbon isotopic composition of leaf	‰
$\delta^{13}C_{air}$	carbon isotopic composition of the atmosphere	‰
a	discrimination due to CO_2 diffusion in air	‰

b	discrimination due to the enzyme Rubisco	‰
d	diffusivity of CO_2 gas in air	mol m^{-3}
v	molar volume of air	m^3 mol^{-1}
*Γ**	CO_2 compensation point in the absence of dark respiration	ppmV

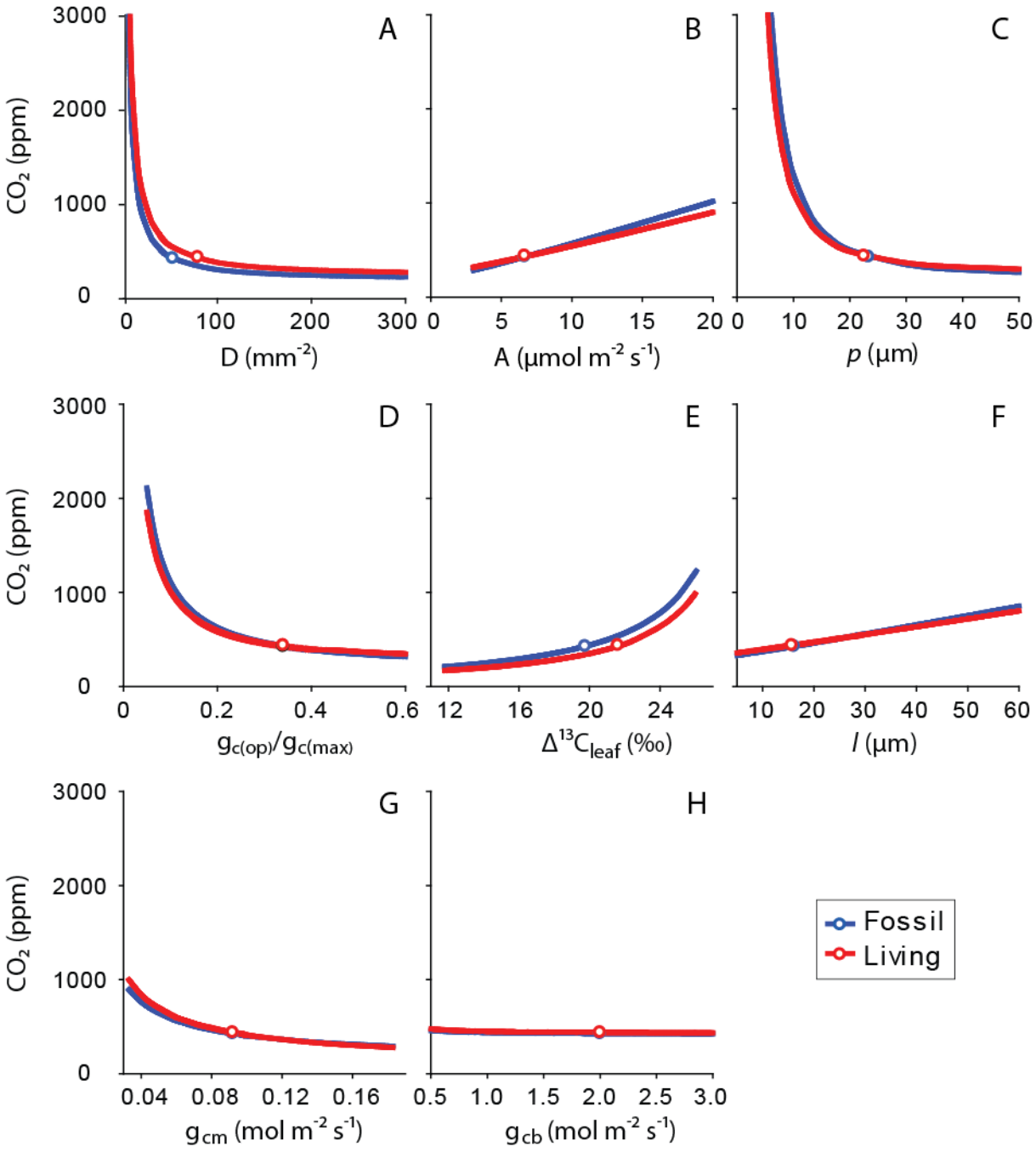

Figure DR3. Sensitivity of input parameters on calculated CO_2 following the Franks et al. (2014) model. The range in all input parameters are representative of C_3 plants. The blue circles are the site-mean values for Napartulik; the red circles are the mean values for extant *Metasequoia*. Along each curve, only one input parameter was varied; all others are held fixed at their measured or modeled means. **A.** D = stomatal density **B.** A = photosynthetic rate **C.** p = pore length **D.** $g_{c(op)}/g_{c(max)}$ = scaling between operational and maximum stomatal conductance **E.** $\Delta^{13}C_{leaf}$ = photosynthetic fractionation **F.** l = stomatal pore depth **G.** g_{cm} = mesophyll conductance **H.** g_{cb} = boundary layer conductance.

DR2.2. Cuticle preparation

All fossils used in this study were collected by D.L.R. during the summer of 1999 (see Fig. DR4 for pictures). Fossil plant cuticle from Napartulik, including that of *Metasequoia occidentalis,* has generally been difficult to prepare for microscopy. Here, a simplified method similar to those of Wang and Leng (2011) and Liu and Basinger (2009) was developed to clear the leaf surface, rather than clearing by dissolving the mesophyll. Our method appears to yield higher quality images than those from previous studies (Fig. DR5). The method requires a three step maceration sequence: 1) 24 hrs in full strength hydrochloric acid (HCl; 12.1 N) to remove any carbonate; 2) 72 hrs in full strength hydrofluoric acid (HF; 28.9 N) to remove a silicate coating on leaves that was commonly observed with elemental mapping under scanning electron microscopy (SEM); 3) 30 s to 5 min in full strength nitric acid (HNO_3; 15.9 N) to loosen an organic film covering many of the leaves. The timing of step three is critical and was stopped when the cuticle changed to a light brown color. Between each step, leaves were thoroughly washed (at least 3×) with distilled water. After maceration, a fine point brush was used to gently remove the loosened organic film from the leaf surface. Leaves were wet mounted and viewed with epifluorescence microscopy.

In one exceptional case, the mesophyll from a single leaf was successfully cleared from fossil layer C. After the HCl and HF treatments, the ends of the leaf and one lateral edge were removed using a razor blade. The leaf was then placed in household bleach for ~3 min to oxidize and clear the mesophyll. The cleared cuticle was mounted in water and viewed in plain transmitted light and epifluorescence (Fig. DR6). Numerous attempts were made to prepare cuticle from all 18 sampled layers, including six layers present on both ridge systems (see Figs. DR1-DR2). However, only six layers were well enough preserved to view clear cellular detail. It should be noted that layers A-E are present on both ridge systems, but the corresponding material used for this study comes exclusively from the Little Ridge (Fig. DR1).

Leaves from extant *M. glyptostroboides* did not require any cuticle preparation; they were wet-mounted directly and viewed with epifluorescence microscopy.

Figure DR4. Images of fossil and living *Metasequoia* leaves. **A.** Fossil litter mats from forest horizon B' at Napartulik. **B.** Fossil *M. occidentalis* leaflets from forest horizon B' at Napartulik. **C.** Living *M. glyptostroboides* leaves. All scale bars = 10 cm.

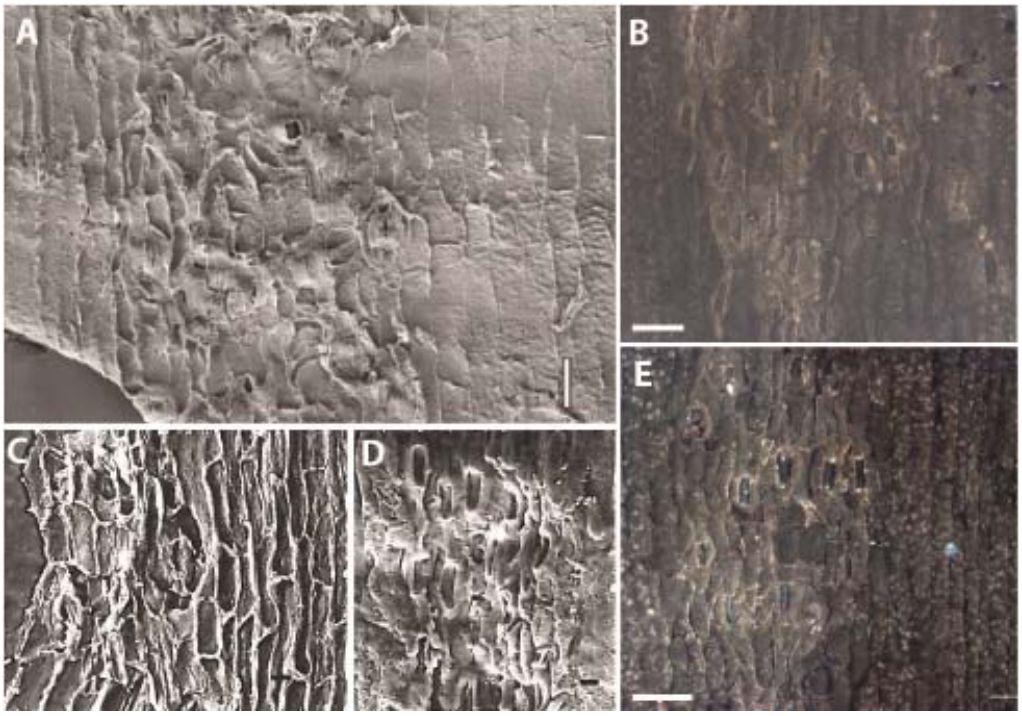

Figure DR5. Comparison of cuticle preps from Napartulik *Metasequoia* using different methodologies. **A.** SEM image of cuticle prep presented in Wang and Leng (2011); scale bar = 30 μm. **B. and E.** Leaf surfaces of *Metasequoia* from fossil forest layer C at Napartulik, obtained using method described here; scale bars = 50 μm. Images taken under epifluorescence. **C. and D.** SEM images of cuticle presented by Liu and Basinger (2009); scale bars = 10 μm.

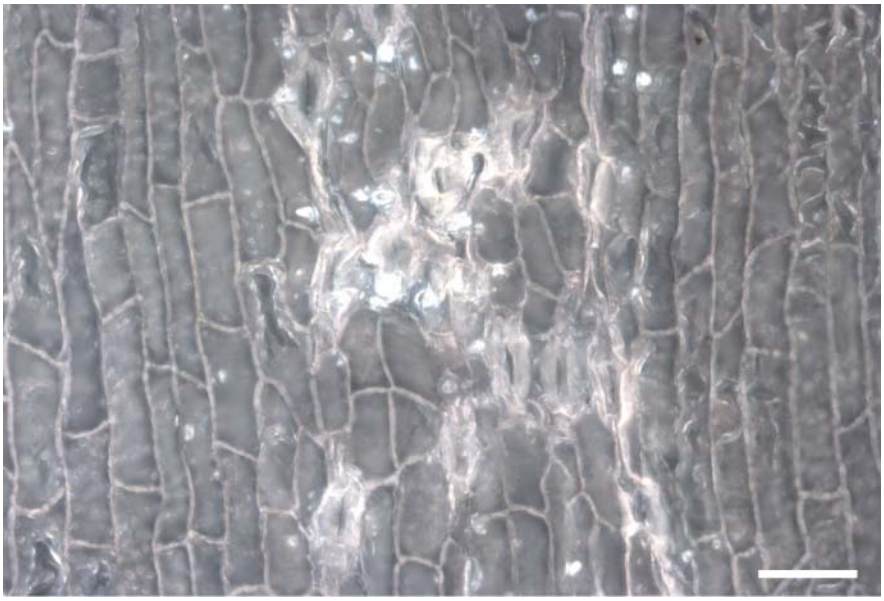

Figure DR6. Cuticle of *M. occidentalis* cleared of mesophyll from Napartulik fossil forest layer C. Image shows internal surface of cuticle under epifluorescence light. Scale bar = 50 μm.

DR2.3. Reconstructing CO_2 from Napartulik *M. occidentalis*

There are three overarching parameters required in the model: A, $g_{c(tot)}$, and C_i/C_a (see eq. DR2). To constrain A and $g_{c(tot)}$, on June 10th, 2012 a total of 12 measurements of net photosynthetic rate (A_0) and leaf conductance to water vapor ($g_{w(op)}$) were taken from an extant *M. glyptostroboides* tree growing on the campus of Wesleyan University, Middletown, CT using a LiCor infrared gas analyzer (Li-6400 system). Chamber conditions were calibrated and maintained at 390 ppm CO_2, 25°C leaf temperature, 1-1.5 kPa leaf-to-air VPD (vapor pressure deficit), and 1000 μmol m^{-2} s^{-1} PAR (photosynthetically active radiation). Measurements were made in the midmorning on leaves growing in full sun. The water supply of the tree was supplemented with 20 gallons of water per day for 4 weeks prior to making measurements to minimize the impact of water stress on photosynthetic rate (Napartulik *Metasequoia* grew near swamps). All measured values were adjusted for area by measuring total projected leaf surface area exposed in the chamber using Image-j software (http://rsbweb.nih.gov/ij/).

The calculation of $g_{c(tot)}$ requires a number of steps. First, values of $g_{w(op)}$ were used to calculate a scaling factor between $g_{c(max)}$ and $g_{c(op)}$. $g_{w(op)}$ was converted to leaf conductance to CO_2 (g_c) by dividing by 1.6, the scaling in diffusion rate between H_2O and CO_2 (Farquhar et al., 1989). Because conductance reported from the Li-6400 system incorporates not only stomatal conductance but also mesophyll conductance, g_{cm}, we removed mesophyll conductance using the following relationship (Franks et al., 2014; Jones, 1992):

$$g_{c(op)} = \frac{1}{\frac{1}{g_c} - \frac{1}{g_{cm}}} \qquad \text{(DR9)}$$

where g_{cm} corresponds to 0.013*A_0 (Franks et al., 2014). For seven measurements of $g_{c(op)}$, a corresponding mean $g_{c(max)}$ value was calculated (described next) from the same leaves (n = 5 leaves per $g_{c(op)}$ value). The mean value and standard error of the mean (s.e.m.) for these seven values was used for scaling present-day and fossil $g_{c(max)}$ values to $g_{c(op)}$. See Table DR2 for list of all physiological inputs and scalings.

Table DR2. Scaling factors and photosynthetic inputs, with associated error. *indicates that error was not measured; in these cases 5% of the scaling value was assumed to encompass 1 standard error of the mean (s.e.m.). Uncertainty in all listed parameters, along with D and $\delta^{13}C$ of the plant and atmosphere, was used to propagate error in the CO_2 estimates. GCW/p was used only for the reconstruction of present-day CO_2 because p cannot be measured from fossils. Units for A_0 are μmol m^{-2} s^{-1}; all other terms are dimensionless.

Parameter	Value	s.e.m.
A_0	6.67	0.39
$g_{c(op)}/g_{c(max)}$	0.34	0.038
p/IRL	0.84	0.0073
GCW/IRL	0.58	0.0093
GCW/p	0.70	0.013
coefficient for a_{max}*	0.5	0.025
GCW/l*	1.0	0.05
g_{cm}/A*	0.013	0.00065

Multiple input parameters are needed to calculate $g_{c(max)}$ (see eq. DR6). D was measured within-band and then adjusted by the percentage of the abaxial leaf surface (*Metasequoia* is hypostomatous) composed of stomatal bands to determine the projected whole-leaf D. For example, if the within-band D is 150 mm^{-2} and the stomatal bands compose 50% of the abaxial leaf surface, then the whole-leaf D is 75 mm^{-2}. Typically for conifers (including *Metasequoia*), whose stomata are arranged in two bands separated by the midvein, D is reported as within-band D (e.g., Doria et al., 2011). For purposes of reconstructing conductance, however, it is more important to know what D is for the entire projected leaf surface because both conductance and A are usually measured on the projected area of the whole leaf. Importantly, if the proportion of the leaf surface composed of stomatal bands changes through time, this would change whole-leaf conductance for a given within-band D or stomatal index and could potentially confound traditional stomatal approaches for reconstructing CO_2. Indeed, the mean fraction of stomatal band tissue in Napartulik *Metasequoia* is 29.0 ± 0.05 % compared to 53.7 ± 0.04 % in living *Metasequoia*.

Maximum stomatal aperture (a_{max}) and pore depth (l) are needed to calculate $g_{c(max)}$. These are typically scaled from guard cell length (see section DR2.1), but guard cell length is difficult to measure in fossil and living *Metasequoia*. This is because overarching cells cover most of the stomatal complex, leaving an inner rectangle that, in the case of poor staining or viewing of cuticle under epifluorescence, can mistakenly appear to be the entire stomatal complex (Fig. DR7). Fortunately, this inner rectangular length (*IRL*) was easily measurable on most fossils, and was the basis for the fossil scalings to p and to GCW (Fig. DR8). In most plants, $GCW = l$ owing to the circular shape of the guard cells in cross-section when fully inflated (Franks and Beerling, 2009a; see also Fig. DR7); following this relationship we assumed

that our modeled *GCW* scaled 1:1 with *l*. We calculated a_{max} from scaled values of *p* assuming that a_{max} is equivalent to half the area of a circle whose diameter is P_l ($a_{max} = 0.5*\pi*(p/2)^2$), a scaling that holds true for most gymnosperms (Beerling and Woodward, 1997; Franks and Beerling, 2009a).

Scaling factors for stomatal geometry were calibrated using archived slides from extant *M. glyptosroboides* saplings grown outside under ambient conditions in Middletown, CT (Doria et al., 2011). All scaling factors are the mean values of $n = 100$ stomata and are listed in Table DR2. To validate the assumed 1:1 relationship between *GCW* and *l* we measured *GCW* and *l* in cross sections from extant *M. glyptostroboides* leaves from the tree on campus at Wesleyan University (see Fig. 7A-C for examples). The observed scaling from these limited measurements (0.88; $n = 7$ stomata) is significantly different from the assumed scaling of 1.0 ($P = 0.003$), however the difference in estimated CO_2 resulting from this difference in scaling is generally <10 ppm (see also Fig. DR3F). Furthermore, the 1:1 scaling assumes fully-inflated guard cells (under tugor), which was likely not true for our leaves because they were preserved only in water (and not fixed immediately after harvest). Finally, our measurements of both *GCW* and *l* may be biased if the stomatal orientations were not exactly orthogonal to our cuts. For these three reasons, we favor the generic scaling value of 1.0 (Franks and Beerling, 2009a).

It is possible that our adopted scalings, which are based on extant plants, were different for Napartulik *Metasequoia*. To address this possibility, we tested in a limited fashion two scalings directly from Napartulik *Metasequoia*. The *IRL* to *p* scaling was tested using especially well-preserved fossils from Layer C; the fossil scaling (0.81) is slightly lower, but significantly different, than the scaling measured from archived saplings from (Doria et al., 2011) (0.84; $P = 0.003$). However, as with the *GCW:l* scaling, this difference is essentially negligible in the final

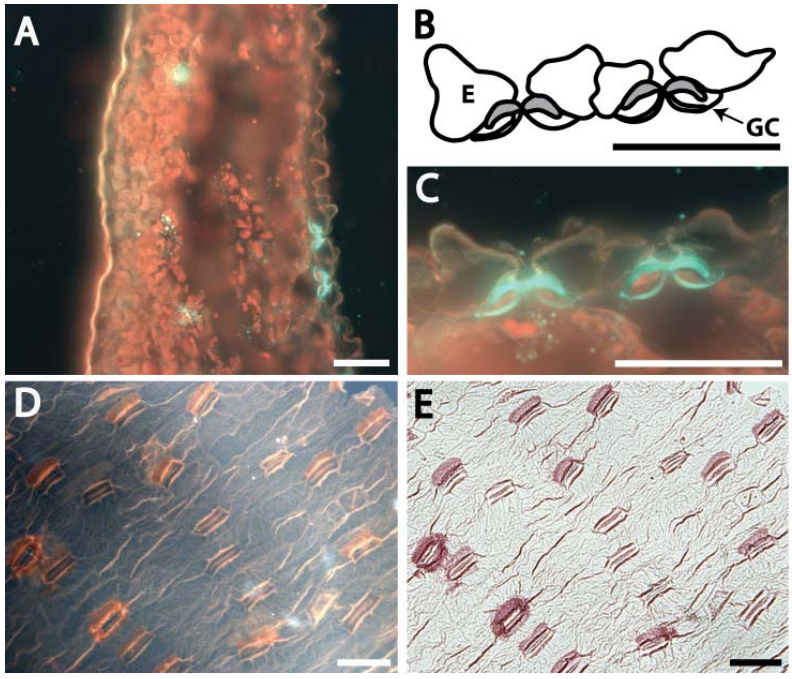

Figure DR7. **A.** Cross section of a mature extant *Metasequoia* leaf showing undulating epidermal cells and uneven cuticle (*sensu* Leng et al., 2001) with stomata overarched by epidermal cells (stomatal complex is bluish-green). **B.**

Illustration of **C** showing close-up of stomata in cross section. Note the subsidiary epidermal cells (labeled E) are overarching the guard cells (GC, colored grey in B, bluish-green in C). **D.** Cleared and stained *Metasequoia* cuticle of a sapling from (Doria et al., 2011) viewed under epifluorescence. **E.** The same cuticle sample and view from D viewed under transmitted light. Note that the inconsistent staining of the guard cells clearly demonstrates that the guard cells are not visible under epifluorescence, especially when not stained. All scale bars = 50 □m.

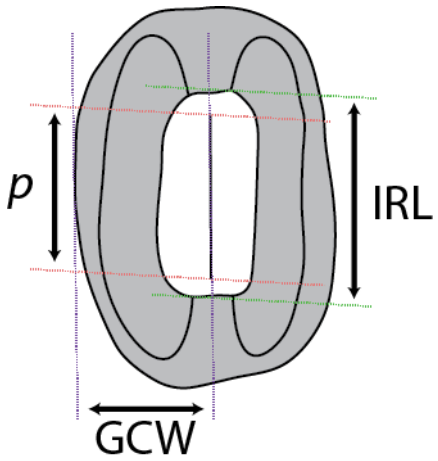

Figure DR8. Illustration of stomatal measurements taken on fossil and living *Metasequoia*. The shaded grey portion represents what is covered by the overarching epidermal cells and not visible in map view using epifluorescence (see Fig. DR7). *p* = pore length. *IRL* = inner rectangular length. *GCW* = single guard cell width. For fossils, *IRL* was most readily accessible to measure and was used to scale to *p* and *GCW*.

CO_2 reconstruction (Fig. DR3C). Additionally, the measured *p* from the fossils likely represents a minimum because it is common for the pore slit to not fully preserve (e.g., Fig. DR5). If our measurements of *p* are too small, this could explain the slightly lower scaling value. For a single fossil stoma where we could measure both *IRL* and *GCW* (from cleared cuticle from Layer C; see Fig. DR6), the observed scaling (0.60) is close to our calibrated scaling (0.58) from the Doria et al. (2011) material. We modified the R code provided by Franks et al. (2014) by replacing guard cell length with *IRL* and its associated scaling.

Measurements of *D* and *IRL* were taken from three fields of view (*IRL* from three stomata per field of view); the leaf mean values were used as the unit of replication in all cases. Sample sizes for reconstructing CO_2 were $n = 10$ leaves per fossil horizon. The scaled values for *l* and a_{max} and the measured *D* were used to calculate $g_{c(max)}$ using eq. DR6, which was then scaled to $g_{c(op)}$ using our scaling of 0.34 from living *Metasequoia*. Other conductance terms were approximated following (Franks et al., 2014) with a constant value of 2 $mol^{-2}\ s^{-1}$ for g_{cb}; g_{cm} is approximated using the scaling 0.013**A* (see Table DR2). Conductance terms were combined in series to reconstruct $g_{c(tot)}$ following eq. DR7.

The C_i/C_a ratio can be reconstructed from the $\delta^{13}C$ of leaf tissue and the atmosphere. $\delta^{13}C_{leaf}$ was analyzed at the University of California Davis Stable Isotope Facility. Their long-term instrumental standard deviation for $\delta^{13}C$ is ±0.2 ‰. Fossil samples were macerated in full strength HCl for 24 hours to remove carbonate, rinsed with distilled water, and dried prior to being sent for analysis. Ten leaves from each fossil layer were analyzed. All reported $\delta^{13}C$ values are relative to the Vienna Pee Dee Belemite (VPD). Carbon isotopic composition of the

atmosphere ($\delta^{13}C_{atm}$) for Napartulik fossils was approximated as -5.75 ± 0.7‰ using the model of Tipple et al. (2010) that is based on a record of benthic foraminifera $\delta^{13}C$. The 0.7‰ error term, which we take as representing 2 s.e.m., comes from the 90% confidence interval presented by (Tipple et al., 2010) and incorporating the likely age range for Napartulik (47.9-37.8 Ma). We used eqs. DR3 and DR4 to reconstruct $\Delta^{13}C_{leaf}$ and C_i/C_a, respectively.

We used the measured values of A_0 (reported in Table DR2) and a reference C_{a0} of 390 ppm to calculate the value of A that accounts for changing C_a by solving eqs. DR2 and DR8 iteratively. The final CO_2 reconstructions are the median values resulting from the Monte Carlo resampling procedure described in the main text.

It is important to note that stomata respond to the partial pressure of CO_2 in air (pCO_2 , Pa) not strictly the mole fraction (ppm) (Woodward, 1986; Woodward and Bazzaz, 1988). Because partial pressure changes with elevation but mole fraction does not, elevation (and paleoelevation) must be controlled for when reconstructing CO_2 from stomatal features. This elevation effect typically becomes important only when above ~1000 m (Beerling and Royer, 2002). All calibration work was done at Wesleyan University, which is near sea level (45 m asl). Napartulik today is at low elevation (~250 m asl), however there are no strong constraints for its paleoelevation during the middle Eocene. Nonetheless, considering the meanderplain depositional environment, the abundance of fine-grained sands and silts at the site, the proximity of the site to the edge of the North American craton, and the lack of structural evidence supporting the presence of an uplift plateau together suggests that the paleoelevation of Napartulik in the middle Eocene was likely < 1000 m asl (Ricketts, 1991, 1994). Therefore, we assume a sea-level equivalency between partial pressure and mole fraction (10 ppm = 1 Pa) and express all reconstructed CO_2 values in ppm units.

DR2.4. Reconstructing CO_2 from living *M. glyptostroboides*

Reconstruction of present-day CO_2 from living *M. glyptostroboides* (Appendix DR3) largely mirrors the methods used to reconstruct ancient CO_2 from Napartulik fossils (for physiological measurements and scalings, see Table DR2), but with the following exceptions. Because pore length (p) is measurable on living *Metasequoia*, it—not *IRL*—was used to scale to *GCW* and to directly compute a_{max}. Sample sizes for D and p measurements are n = 35 leaves and for $\delta^{13}C_{leaf}$, n = 10 leaves. Measurements of leaf physiology (described in the previous section), stomatal geometry, and $\delta^{13}C_{leaf}$ each come from the same set of leaves.

For estimating $\delta^{13}C_{air}$ and CO_2 concentration in Middletown, CT, a combination of data from Mauna Loa Observatory, Hawaii (Station MLO, NOAA) and Harvard Forest, Petersham, Massachusetts (http://harvardforest.fas.harvard.edu:8080/exist/xquery/data.xq?id=hf004) were used. Harvard Forest is ~140 km north of Middletown, CT. Seasonal fluctuations in CO_2 concentration and $\delta^{13}C_{air}$ are typically amplified with latitude and therefore it should be expected that seasonal changes at Harvard Forest are larger than at Mauna Loa, which is indeed the case when comparing monthly concentration data from 2008-2010 (Fig. DR9). However, during the months of May and June differences between the two sites are generally <5ppm (indicated by grey bars in Fig. DR9). Therefore the concentration of CO_2 during June, 2012 (the month

physiological measurements were made) from Mauna Loa, 396 ppm, should serve as a robust value for Middletown, CT. For constraining $\delta^{13}C_{air}$, we compiled MLO records of CO_2 concentration and $\delta^{13}C_{air}$ for the months of May and June from 1990-2010 (excluding 1994 when no $\delta^{13}C_{air}$ data are reported) to create a mixing line relating $\delta^{13}C_{air}$ to $1/[CO_2]$ (Fig. DR10). We restricted the analysis to these months because most of the carbon measured for our $\delta^{13}C_{leaf}$ was fixed during May and June of 2012. A value of -8.53‰ for $\delta^{13}C_{air}$ was calculated for June 2012 using the regression equation in Fig. DR10 and assuming a concentration value of 396 ppm; an uncertainty of 0.2‰ was assumed to represent 2 s.e.m. (note: 2 s.e.m. from the regression = 0.026‰, so our assumed error is highly conservative).

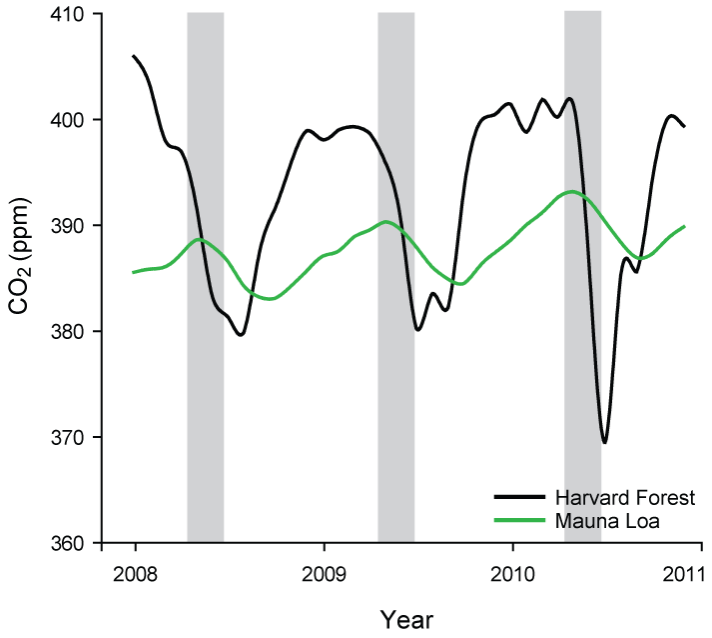

Figure DR9. Average monthly CO_2 concentrations from 2008-2010 from Harvard Forest, Petersham, Massachusetts (black line) and Mauna Loa Observatory, Hawaii (green line). As expected, seasonal variation in CO_2 is amplified at Harvard Forest. However, during May and June, indicated by vertical grey bars, the concentrations of CO_2 from Harvard Forest and Mauna Loa converge. Harvard Forest data are from the hf004-01 data set freely available from http://harvardforest.fas.harvard.edu. Mauna Loa data are the raw monthly average values not corrected for seasonal variation available from http://www.esrl.noaa.gov/gmd/ccgg/trends/.

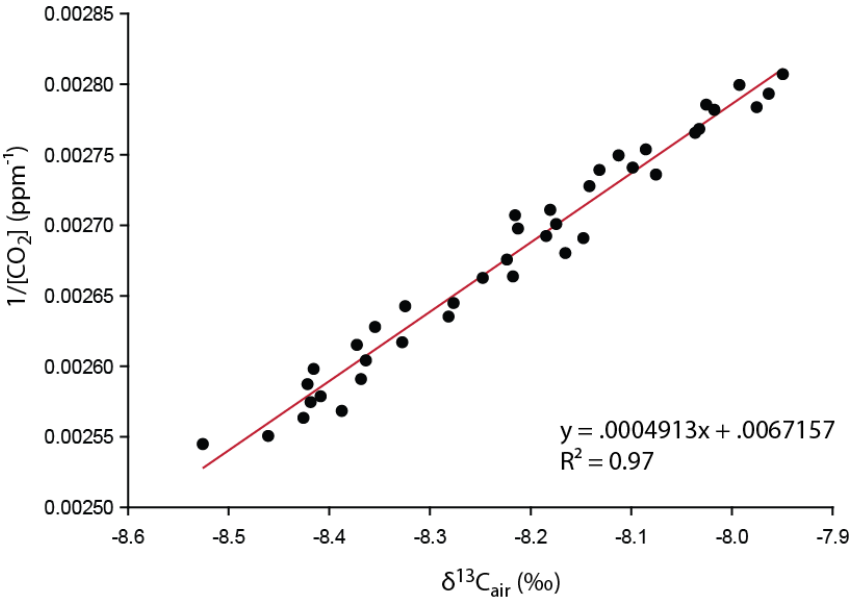

Figure DR10. Keeling plot showing the relationship between $\delta^{13}C_{air}$ and $1/[CO_2]$ for the months of May and June during the years 1990-2010 from Mauna Loa Observatory, Hawaii. Regression equation shown was used to calculate the $\delta^{13}C_{air}$ for June 2012 in Middletown, CT using the June 2012 concentration data from Mauna Loa. Data for the concentration and $\delta^{13}C_{air}$ from Mauna Loa from http://www.esrl.noaa.gov/gmd/ccgg/trends.

APPDENIX DR3. MODEL VALIDATION WITH EXTANT *METASEQUOIA*

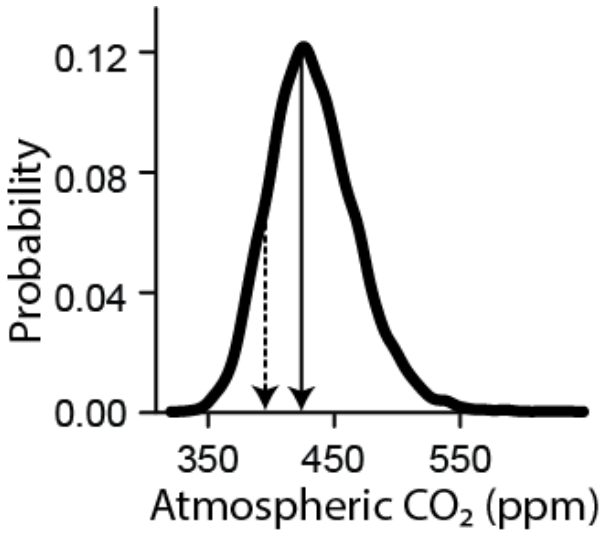

Figure DR11. Probability density function (PDF) for reconstruction of present-day CO_2 from extant *M. glyptostroboides* following the gas-exchange approach of Franks et al. (2014). Reconstructed median value indicated by solid black arrow (445 ppm) and current atmospheric CO_2 taken for June 2012 at Mauna Loa Observatory (396 ppm) indicated by dashed arrow. The close agreement of the reconstructed vs. observed CO_2 values using extant *M. glyptostroboides* (12% error) validates our application of the model to fossil *M. occidentalis* from Napartulik.

APPENDIX DR4. RAW DATA

Table DR3. CO_2 estimates for all fossil layers, site mean (SM), and present-day reconstructions, along with associated $\delta^{13}C$ and stomatal geometry data. Variables are defined in Table DR1. s.e.m. = standard error of the mean. Lower bound = 2.5 percentile; upper bound = 97.5 percentile.

	CO_2 (ppm)	lower bound (ppm)	upper bound (ppm)	$\delta^{13}C$ (‰)	s.e.m. (‰)	$\Delta^{13}C_{leaf}$ (‰)	C_i/C_a	*p* (µm)	s.e.m. (µm)
B'	409	346	499	25.35	0.12	20.11	0.61	23.14	
A	417	347	526	25.19	0.11	19.94	0.61	23.65	
C	440	370	546	25.34	0.16	20.10	0.61	23.97	
D	392	328	483	24.38	0.12	19.09	0.57	24.44	
E	424	346	535	24.63	0.41	19.36	0.58	22.38	
F	473	395	589	25.19	0.12	19.94	0.61	22.09	
SM	424	359	513	25.01	0.09	19.76	0.60	23.28	
Modern	430	373	509	29.44	0.16	21.55	0.67	22.52	0.21

	D (mm^{-2})	s.e.m. (mm^{-2})	IRL (µm)	s.e.m. (µm)	*l* (µm)	a_{max} (m^2)	g_{cmax} (mol m^{-2} s^{-1})	g_{cop} (mol m^{-2} s^{-1})	g_{cm} (mol m^{-2} s^{-1})	$g_{c(tot)}$ (mol m^{-2} s^{-1})
B'	60.0	3.9	27.55	0.48	15.98	2.10E-10	0.257	0.087	0.088	0.0429
A	55.2	5.3	28.16	0.48	16.33	2.19E-10	0.242	0.082	0.088	0.0417
C	51.0	3.2	28.54	0.42	16.55	2.25E-10	0.227	0.077	0.090	0.0406
D	50.5	3.3	29.10	0.30	16.88	2.34E-10	0.229	0.078	0.087	0.0402
E	50.8	2.8	26.65	0.77	15.46	1.96E-10	0.211	0.072	0.089	0.0389
F	48.0	1.5	26.29	0.63	15.25	1.91E-10	0.196	0.067	0.091	0.0378
SM	52.6	0.1	27.71	0.25	16.07	2.18E-10	0.227	0.077	0.089	0.0404
Modern	79.1	1.5			15.72	1.99E-10	0.328	0.112	0.089	0.0483

APPENDIX DR5. RECONSTRUCTION OF CO_2 USING STOMATAL INDEX

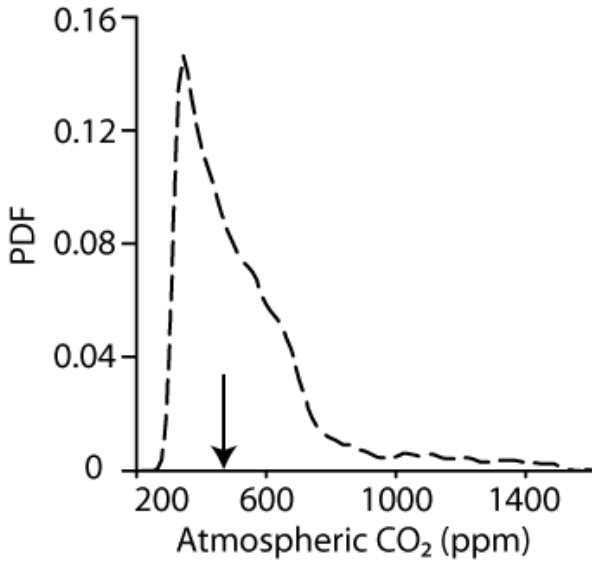

Figure DR12. Probability density function (PDF) for the stomatal index-based reconstruction of CO_2 from fossil forest layer C at Napartulik, following the resampling protocol of (Beerling et al., 2009). Median value indicated by black arrow (471 ppm). We did not count epidermal cells that were overarching the stomatal complex (Fig. DR7), which is consistent with how epidermal cells were counted for the *Metasequoia* calibration function (Doria et al., 2011). Paleobotanists typically consider extant ***M. glyptostroboides*** to be conspecific with fossil ***M. occidentalis*** (LePage et al., 2005; Liu and Basinger, 2009), validating the use of this traditional approach.

REFERENCES

Basinger, J. F., 1991, The fossil forests of the Buchanan Lake Formation (early Tertiary), Axel Heiberg Island, Canadian Arctic Archipelago: Preliminary floristics and paleoclimate, *in* Christie, R. L., and McMillian, N. J., eds., Tertiary fossil forests of the Geodetic Hills Axel Heiberg Island, Arctic Archipelago: Geological Survey of Canada Bulletin 403, p. 39-65.

Beerling, D. J., and Royer, D. L., 2002, Fossil plants as indicators of the Phanerozoic global carbon cycle: Annual Review of Earth and Planetary Sciences, v. 30, p. 527-556.

Beerling, D. J., and Woodward, F. I., 1997, Changes in land plant function over the Phanerozoic: reconstructions based on the fossil record: Botanical Journal of the Linnean Society, v. 124, p. 137-153.

Beerling, D. J., Fox, A., and Anderson, C. W., 2009, Quantitative uncertainty analyses of ancient atmospheric CO_2 estimates from fossil leaves: American Journal of Science, v. 309, p. 775-787.

Doria, G., Royer, D. L., Wolfe, A. P., Fox, A., Westgate, J. A., and Beerling, D. J., 2011, Declining atmospheric CO_2 during the late Middle Eocene climate transition: American Journal of Science, v. 311, p. 63-75.

Eberle, J. J., and Greenwood, D. R., 2012, Life at the top of the greenhouse Eocene world—A review of the Eocene flora and vertebrate fauna from Canada's high Arctic: Geological Society of America Bulletin, v. 124, p. 3-23.

Eberle, J. J., and Storer, J. E., 1999, Northernmost record of brontotheres, Axel Heiberg Island, Canada: Implications for age of the Buchanan Lake Formation and brontothere paleobiology: Journal of Paleontology, v. 73, p. 979-983.

Erdei, B., Utescher, T., Hably, L., Tamás, J., Roth-Nebelsick, A., and Grein, M., 2012, Early Oligocene continental climate of the Palaeogene Basin (Hungary and Slovenia) and the surrounding area: Turkish Journal of Earth Sciences, v. 21, p. 153-186.

Farquhar, G. D., and Richards, R. A., 1984, Isotopic composition of plant carbon correlates with water-use efficiency of wheat genotypes: Functional Plant Biology, v. 11, p. 539-552.

Farquhar, G. D., and Sharkey, T. D., 1982, Stomatal conductance and photosynthesis: Annual Review of Plant Physiology, v. 33, p. 317-345.

Farquhar, G. D., Ehleringer, J. R., and Hubick, K. T., 1989, Carbon isotope discrimination and photosynthesis: Annual Review of Plant Physiology and Plant Molecular Biology, v. 40, p. 503-537.

Farquhar, G. D., O'Leary, M. H., and Berry, J. A., 1982, On the relationship between carbon isotope discrimination and the intercellular carbon dioxide concentration in leaves: Functional Plant Biology, v. 9, p. 121-137.

Franks, P. J., and Beerling, D. J., 2009a, CO_2-forced evolution of plant gas exchange capacity and water-use efficiency over the Phanerozoic: Geobiology, v. 7, p. 227-236.

Franks, P. J., and Beerling, D. J., 2009b, Maximum leaf conductance driven by CO_2 effects on stomatal size and density over geologic time: Proceedings of the National Academy of Sciences USA, v. 106, p. 10343-10347.

Franks, P. J., Drake, P. L., and Beerling, D. J., 2009, Plasticity in maximum stomatal conductance constrained by negative correlation between stomatal size and density: an analysis using *Eucalyptus globulus*: Plant, Cell & Environment, v. 32, p. 1737-1748.

Franks, P. J., Royer, D. L., Beerling, D. J., Van de Water, P. K., Cantrill, D. J., and Berry, J. A., 2014, New constraints on atmospheric CO_2 concentration for the Phanerozoic: Geophysical Research Letters, v. 41, p. 4685-4694, doi: 10.1002/2014GL060457.

Gradstein, F. M., Ogg, J. G., Schmitz, M. D., and Ogg, G. M., 2012, The Geologic Time Scale 2012: Boston, Elsevier, 1144 p.

Greenwood, D. R., and Basinger, J. F., 1993, Stratigraphy and floristics of Eocene swamp forests from Axel Heiberg Island, Canadian Arctic Archipelago: Canadian Journal of Earth Sciences, v. 30, p. 1914-1923.

Grein, M., Konrad, W., Wilde, V., Utescher, T., and Roth-Nebelsick, A., 2011, Reconstruction of atmospheric CO_2 during the early middle Eocene by application of a gas exchange model to fossil plants from the Messel Formation, Germany: Palaeogeography, Palaeoclimatology, Palaeoecology, v. 309, p. 383-391.

Grein, M., Oehm, C., Konrad, W., Utescher, T., Kunzmann, L., and Roth-Nebelsick, A., 2013, Atmospheric CO_2 from the late Oligocene to early Miocene based on photosynthesis data and fossil leaf characteristics: Palaeogeography, Palaeoclimatology, Palaeoecology, v. 374, p. 41-51.

Harrison, J. C., Mayr, U., McNeil, D. H., Sweet, A. R., McIntyre, D. J., Eberle, J. J., Harington, C. R., Chalmers, J. A., Dam, G., and Nøhr-Hansen, H., 1999, Correlation of Cenozoic sequences of the Canadian Arctic region and Greenland; implications for the tectonic history of northern North America: Bulletin of Canadian Petroleum Geology, v. 47, p. 223-254.

Helliker, B. R., and Richter, S. L., 2008, Subtropical to boreal convergence of tree-leaf temperatures: Nature, v. 454, p. 511-514.

Jahren, A. H., 2007, The Arctic forest of the middle Eocene: Annual Review of Earth and Planetary Sciences, v. 35, p. 509-540.

Jahren, A. H., and Sternberg, L. S. L., 2008, Annual patterns within tree rings of the Arctic middle Eocene (ca. 45 Ma): Isotopic signatures of precipitation, relative humidity, and deciduousness: Geology, v. 36, p. 99.

Jahren, A. H., Byrne, M. C., Graham, H. V., Sternberg, L. S. L., and Summons, R. E., 2009, The environmental water of the middle Eocene Arctic: Evidence from δD, $\delta^{18}O$ and $\delta^{13}C$ within specific compounds: Palaeogeography, Palaeoclimatology, Palaeoecology, v. 271, p. 96-103.

Jahren, A. H., LePage, B. A., and Werts, S. P., 2004, Methanogenesis in Eocene Arctic soils inferred from $\delta^{13}C$ of tree fossil carbonates: Palaeogeography, Palaeoclimatology, Palaeoecology, v. 214, p. 347-358.

Jones, H. G., 1992, Plants and microclimate: A quantitative approach to environmental plant physiology: New York, Cambridge University Press, 428 p.

Kleiss, B., 1996, Sediment retention in a bottomland hardwood wetland in eastern Arkansas: Wetlands, v. 16, p. 321-333.

Kojima, S., Sweda, T., LePage, B. A., and Basinger, J. F., 1998, A new method to estimate accumulation rates of lignites in the Eocene Buchanan Lake Formation, Canadian Arctic: Palaeogeography Palaeoclimatology Palaeoecology, v. 141, p. 115-122.

Konrad, W., Roth-Nebelsick, A., and Grein, M., 2008, Modelling of stomatal density response to atmospheric CO_2: Journal of Theoretical Biology, v. 253, p. 638-658.

Leng, Q., Yang, H., Yang, Q., and Zhou, J., 2001, Variation of cuticle micromorphology of *Metasequoia glyptostroboides* (Taxodiaceae): Botanical Journal of the Linnean Society, v. 136, p. 207-219.

LePage, B. A., 1993, The evolutionary history of *Larix, Picea,* and *Pseudolarix* (Pinaceae) based on fossils from the Buchanan Lake Formation, Axel Heiberg Island, N.W.T., Arctic Canada [Ph.D. Thesis]: University of Saskatchewan, 231 p.

LePage, B. A., Yang, H., and Matsumoto, M., 2005, The evolution and biogeographic history of *Metasequoia*, *in* LePage, B. A., Williams, C. J., and Yang, H., eds., The Geobiology and Ecology of *Metasequoia*: Dordrecht, Netherlands, Springer, p. 3-114.

Liu, C., and Basinger, J. F., 2009, *Metasequoia* Hu et Cheng (Cupressaceae) from the Eocene of Axel Heiberg Island, Canadian High Arctic: Palaeontographica Abt. B, v. 282, p. 69-97.

McIntyre, D. J., 1991, Pollen and spore flora of an Eocene forest, eastern Axel Heiberg Island, N.W.T., *in* Christie, R. L., and McMillian, N. J., eds., Tertiary fossil forests of the Geodetic Hills Axel Heiberg Island, Arctic Archipelago: Geological Survey of Canada Bulletin 403, p. 83-97.

Miall, A. D., 1986, The Eureka Sound Group (Upper Cretaceous-Oligocene), Canadian Arctic Islands: Bulletin of Canadian Petroleum Geology, v. 34, p. 240-270.

Richter, S. L., and LePage, B. A., 2005, A high-resolution palynological analysis, Axel Heiberg Island, Canadian High Arctic, *in* LePage, B. A., Williams, C. J., and Yang, H., eds., The Geobiology and Ecology of *Metasequoia*: Dordrecht, Netherlands, Springer, p. 137-158.

Ricketts, B. D., 1986, New formations in the Eureka Sound Group, Canadian Arctic Islands: Geological Survey of Canada, v. 86-1B, p. 363-374.

Ricketts, B. D., 1991, Sedimentation, Eurekan tectonism and the fossil forest succession on eastern Axel Heiberg Island, Canadian Arctic Archipelago, *in* Christie, R. L., and McMillian, N. J., eds., Tertiary Fossil Forests of the Geodetic Hills Axel Heiberg Island, Arctic Archipelago: Geological Survey of Canada Bulletin 403, p. 1-27.

Ricketts, B. D., 1994, Basin analysis, Eureka Sound Group, Axel Heiberg and Ellesmere Islands, Canadian Arctic Archipelago: Geological Survey of Canada Memoir 439, 119 p.

Ricketts, B. D., and McIntyre, D. J., 1986, The Eureka Sound Group of eastern Axel Heiberg Island: New data on the Eurekan Orogeny: Geological Survey of Canada, v. 86-1B, p. 405-410.

Song, X., Barbour, M. M., Saurer, M., and Helliker, B. R., 2011, Examining the large-scale convergence of photosynthesis-weighted tree leaf temperatures through stable oxygen isotope analysis of multiple data sets: New Phytologist, v. 192, p. 912-924.

Tipple, B. J., Meyers, S. R., and Pagani, M., 2010, Carbon isotope ratio of Cenozoic CO_2: a comparative evaluation of available geochemical proxies: Paleoceanography, v. 25, PA3202, doi:3210.1029/2009PA001851.

Wang, L., and Leng, Q., 2011, A new method to prepare clean cuticular membrane from fossil leaves with thin and fragile cuticles: Science China Earth Sciences, v. 54, p. 223-227.

Williams, C. J., Johnson, A. H., LePage, B. A., Vann, D. R., and Sweda, T., 2003, Reconstruction of Tertiary *Metasequoia* forests. II. Structure, biomass, and productivity of Eocene floodplain forests in the Canadian Arctic: Paleobiology, v. 29, p. 271-292.

Woodward, F. I., 1986, Ecophysiological studies on the shrub *Vaccinium myrtillus* L. taken from a wide altitudinal range: Oecologia, v. 70, p. 580-586.

Woodward, F. I., and Bazzaz, F. A., 1988, The responses of stomatal density to CO_2 partial pressure: Journal of Experimental Botany, v. 39, p. 1771-1781.

Yang, H., Huang, Y., Leng, Q., LePage, B. A., and Williams, C. J., 2005, Biomolecular preservation of Tertiary *Metasequoia* fossil lagerstätten revealed by comparative pyrolysis analysis: Review of Palaeobotany and Palynology, v. 134, p. 237-256.